Inelastic Scattering Dynamics of Ar from a Perfluorinated Self-Assembled Monolayer Surface †

8 AUTHORS, INCLUDING:

Saulo A Vázquez
University of Santiago de Compostela
90 PUBLICATIONS **1,045** CITATIONS

SEE PROFILE

Emilio Martinez-Nuñez
University of Santiago de Compostela
85 PUBLICATIONS **1,019** CITATIONS

SEE PROFILE

Inelastic Scattering Dynamics of Ar from a Perfluorinated Self-Assembled Monolayer Surface[†]

Saulo A. Vázquez,[‡] John R. Morris,[£] Asif Rahaman,[§] Oleg A. Mazyar,[§] Grigoriy Vayner,[§] Srirangam V. Addepalli,[#] William L. Hase,*,[§] and Emilio Martínez-Núñez*,[‡]

Departamento de Química Física, Universidad de Santiago de Compostela, 15782 Santiago de Compostela, Spain, Department of Chemistry, Virginia Tech, Blacksburg, Virginia 24061, Department of Chemistry and Biochemistry, Texas Tech University, Lubbock, Texas 79409, and High Performance Computing Center, Texas Tech University, Lubbock, Texas 79409

Dynamics of Ar atom collisions with a perfluorinated alkanethiol self-assembled monolayer (F-SAM) surface on gold were investigated by classical trajectory simulations and atomic beam scattering techniques. Both explicit-atom (EA) and united-atom (UA) models were used to represent the F-SAM surface; in the UA model, the CF_3 and CF_2 units are represented as single pseudoatoms. Additionally the nonbonded interactions in both models are different. The simulations show the three limiting mechanisms expected for collisions of rare gas atoms (or small molecules) with SAMs, that is, direct scattering, physisorption, and penetration. Surface penetration results in a translational energy distribution, $P(E_f)$, that can be approximately fit to the Boltzmann for thermal desorption, suggesting that surface accommodation is attained to a large extent. Fluorination of the alkanethiol monolayer leads to less energy transfer in Ar collisions. This results from a denser and stiffer surface structure in comparison with that of the alkanethiol SAM, which introduces constraints for conformational changes which play a significant role in the energy-transfer process. The trajectory simulations predict $P(E_f)$ distributions in quite good agreement with those observed in the experiments. The results obtained with the EA and UA models are in reasonably good agreement, although there are some differences.

I. Introduction

Self-assembled monolayers (SAMs) of thiolates on metals are widely used in nanoscience and nanotechnology.[1] They are also very valuable materials for exploring the dynamics of collisions of gases with organic surfaces because their highly ordered and well-characterized structures simplify the elucidation of the microscopic mechanisms of energy transfer. The first gas-surface scattering study involving SAMs was reported by Cohen et al.,[2] who measured the fraction of translational energy transferred in collisions of monatomic and diatomic gases with long-chain, amphiphilic monolayers. They found a correlation between the extent of energy transfer and the rigidity of the chains and the gas/surface mass ratio. In addition, they suggested that the internal rotation of the terminal methyl groups and the concerted waving motion of chains perpendicular to the carbon skeleton play a significant role in the energy transfer.

Since the publication of the above study by Cohen et al.,[2] numerous experimental and theoretical investigations have explored energy transfer in collisions of gas-phase species with SAM surfaces[3−25] and liquid surfaces such as perfluorinated polyether.[26−31] These investigations show that three limiting types of events, direct impulsive scattering, physisorption, and penetration, can take place upon collision. Direct impulsive

scattering refers to the process in which the projectile rebounds directly from the surface after a single encounter.[32−35] Physisorption occurs when the gas species is adsorbed on the surface for a substantial period of time. Physisorption together with penetration into the monolayer have often been classified as trapping desorption (TD).[35−37]

Because of the inherent difficulty to directly observe trapping desorption, the common experimental practice[2−6,32−38] is to equate the fraction of TD to the fraction of the translational energy distribution of the scattered species, $P(E_f)$, that can be fit to a Maxwell−Boltzmann distribution for thermal desorption,[39] that is

$$P(E_f) = (k_B T_s)^{-2} E_f \exp(-E_f/k_B T_s) \tag{1}$$

where k_B is Boltzmann's constant, E_f is the final translational energy of the scattered gas particle, and T_s is the surface temperature. The remaining higher-energy component of the distribution is then assigned to inelastic scattering. However, there are uncertainties in this approach since classical trajectory simulations of Ne scattering off SAMs adsorbed on $Au\{1,1,1\}$ have shown that a Boltzmann component in $P(E_f)$ does not necessarily arise from a trapping desorption intermediate.[10−13] A substantial number of trajectories associated with this component come from single-bounce encounters. Moreover, the low-energy component of the $P(E_f)$ distribution may be fit by an effective surface temperature that differs from the actual temperature of the surface. In many instances, this effective temperature is significantly higher than T_s, which may be interpreted in terms of thermalization with a subset of surface

vibrational modes.[13] In a similar vein, the fraction of the Boltzmann component in $P(E_f)$ for CO_2 scattering off of the F-SAM surface is not equivalent to either the fraction of physisorption or penetration events, or their combination.[21]

Most of the above experimental and theoretical studies are concerned with inelastic scattering of rare-gas atoms (especially Ne and Ar) with alkanethiol SAMs on gold.[4-15] The use of rare gases at low collision energies facilitates the interpretation of the experimental observations as well as the use of computer simulations because it removes complications from chemical reaction. Nevertheless, the variety of projectile species investigated so far is quite wide, ranging from open-shell atoms [especially $O(^3P)$][18-20] and small molecules (e.g., O_2, NO, CO_2, aniline, $SiMe_3^+$)[2,3,21-23] to chemical species as large as peptide ions.[24,25]

Several studies have been designed to probe gas-surface adsorption[40-42] and the dynamics of energy transfer and thermal accommodation[4,16,17] in collisions of gases with functionalized SAMs surfaces. These investigations are important to understand the role of the surface structure in the energy-transfer dynamics. In particular, it was found that the extent of thermalization and the percentage of energy transferred to the surface (using Ar as the projectile gas) decreases when the alkanethiol chains of SAMs on gold contain hydrogen-bonding groups at the terminus, such as −OH, −COOH, and −NH$_2$.[4,16,17] When the hydrogen-bonding groups are buried beneath the methyl terminus, the experiments show that impulsive scattering decreases and accommodation increases as the functional group is located farther below the methyl terminus.[17] The scattering dynamics becomes similar to that of *n*-alkanethiol SAMs when the H-bonding groups are positioned below five or six methylene groups. This fact is related to the observation that, for high-energy Ar collisions on *n*-alkanethiol SAMs on gold, long-range molecular motions involving up to six carbon atoms along the individual chains play the dominant role in the energy-transfer dynamics.[6]

In the present work, we report the results of classical trajectory simulations of Ar collisions with a perfluorinated alkanethiol [$CF_3(CF_2)_7S$] self-assembled monolayer (F-SAM) on gold, at collisions energies of 50 and 100 kJ/mol. The general aim of the present work is to extend the previous investigations of the dynamics of Ar scattering from SAMs surfaces and analyze the effect of fluorination on the energy-transfer dynamics. The simulations were performed with two model potentials for the F-SAM surface, an explicit-atom (EA) model, used with success in a recent dynamics study of CO_2 scattering from the F-SAM,[21] and a united-atom (UA) model, wherein the CF_3 and CF_2 units are represented as single pseudoatoms. As a complement to the trajectory simulations, we carried out atomic beam scattering experiments to determine translational energy distributions of the scattered Ar atoms. The comparison between the experimental and the trajectory translational energy distributions will serve to judge the reliability of the present simulations. A specific goal of this study is to assess the performance of the UA model, given that this model may be very useful for large-scale computations because it reduces the CPU time considerably in comparison with that of the EA model.

II. Computational Details

A. Potential Energy Surfaces. The potential energy function employed to study the dynamics of inelastic collisions of Ar with the F-SAM surface comprises a potential for the surface (V_{surf}) plus an Ar/F-SAM interaction term ($V_{Ar,surf}$)

$$V = V_{surf} + V_{Ar-surf} \tag{2}$$

As indicated above, both explicit-atom and united-atom models were considered to represent the F-SAM. In the EA model, developed in previous work,[43] the F-SAM consists of 48 chains of the $CF_3(CF_2)_7S$ radical adsorbed on a single layer of 225 Au atoms held fixed at their equilibrium positions. The validity of treating the gold atoms as a rigid anchoring slab has been shown elsewhere.[12] The S atoms are adsorbed in a shape of a rhombus, to correspond to experiment,[44] with each S atom interacting with the closest three Au atoms via three individual harmonic stretching potentials.[45]

The potential energy function of the explicit-atom F-SAM surface[43] comprises a sum of nonbonded interactions between atoms from different $C_8F_{17}S$ chains, $V^{NB}(r_{ij})$, as well as energy contributions due to the distortions of bonds, $V^S(r_{ij})$, bond angles, $V^B(\theta_{ijk})$, and torsion angles, $V^T(\varphi_{ijkl})$

$$V_{F-SAM} = \sum_{i<j} V^{NB}(r_{ij}) + \sum_{i,j} V^S(r_{ij}) +$$
$$\sum_{i,j,k} V^B(\theta_{ijk}) + \sum_{i,j,k,l} V^T(\varphi_{ijkl}) \tag{3}$$

The stretching and bending interactions for atoms *i*, *j*, and *k* are modeled by harmonic functions

$$V^S(r_{ij}) = 0.5k_{\alpha\beta}^S(r_{ij} - r_{\alpha\beta}^0)^2 \tag{4}$$

$$V^B(\theta_{ijk}) = 0.5k_{\alpha\beta\gamma}^B(\theta_{ijk} - \theta_{\alpha\beta\gamma}^0)^2 \tag{5}$$

where $r_{\alpha\beta}^0$ is the equilibrium bond length for atom types α and β; $\theta_{\alpha\beta\gamma}^0$ is the equilibrium bond angle for atom types α, β, and γ; and $k_{\alpha\beta}^S$ and $k_{\alpha\beta\gamma}^B$ are the stretching and bending force constants, respectively. The torsional terms are given by cosine series

$$V^T = \sum_n 0.5k_{n,\alpha\beta\gamma\delta}^T(1 - \cos(n\varphi - \varphi_{n,\alpha\beta\gamma\delta}^0)) \tag{6}$$

where $k_{n,\alpha\beta\gamma\delta}^T$ and $\varphi_{n,\alpha\beta\gamma\delta}^0$ are torsional parameters. The nonbonded interactions in the EA model are modeled by Buckingham potentials

$$V^{NB}(r_{ij}) = A_{\alpha\beta} \exp(-B_{\alpha\beta}r_{ij}) + \frac{C_{\alpha\beta}}{r_{ij}^{D\alpha\beta}} \tag{7}$$

where $A_{\alpha\beta}$, $B_{\alpha\beta}$, $C_{\alpha\beta}$, and $D_{\alpha\beta}$ are the Buckingham parameters for atom types α and β. As seen below, the nonbonded interactions for the UA model of the surface are different. All of the parameters for the EA model of the F-SAM surface are given in ref 37. This EA model gives a structure for the F-SAM[21] which is in good agreement with experiment;[44] for example, the $C_8F_{17}S$ chains form a tilt angle of 13.7° with respect to the Au normal compared with the experimental value of 12 ± 2°,[44] and the average distance between the terminal C atoms is 6.247 ± 0.808 Å in comparison with the experimental value of 5.780 ± 0.001 Å.[44]

The interaction term between Ar and the F-SAM surface in the EA model is also expressed by a series of pairwise Buckingham terms, with $D = 6$. Parameters A, B, and C for the Ar···C and Ar···F interaction potentials were obtained elsewhere[46] by accurate fits to ab initio potentials of Ar + CF_4 calculated at the CCSD(T)/aug-cc-pVTZ level with counterpoise corrections for basis set superposition errors. These potentials are also in excellent agreement with very recent ab initio

Scattering Dynamics of Ar from a F-SAM Surface

J. Phys. Chem. A, Vol. 111, No. 49, 2007 **12787**

TABLE 1: Parameters Employed in the Potential Energy Surface of the UA Model

bond force-filed parameters		
bond type[a]	k^S (mdyn/Å)	r^0 (Å)
Au−S	2.8	b
S−CF₂	5.7	1.82
CF₂−CF₂, CF₂−CF₃	3.51[c]	1.53[d]

bond angle force-field parameters		
bend type[e,f]	k^B (kcal/mol·rad²)	θ^0 (deg)
S−CF₂−CF₂, CF₂−CF₂−CF₂, CF₂−CF₂−CF₃	0.863	114.6

torsion force-field parameters			
torsional type[e,f]	n	k^T (kcal/mol)	φ^0 (deg)
S−CF₂−CF₂−CF₂	1	7.08471554	0.0
CF₂−CF₂−CF₂−CF₂	2	4.208465094	0.0
CF₂−CF₂−CF₂−CF₃	3	5.462568782	0.0
	4	2.953659654	0.0
	5	1.726793568	0.0
	6	1.726793568	0.0
	7	0.2560869246	−180.0

nonbonded force-field parameters		
UA pair[f]	A (kcal/mol Å¹²)	B (kcal/mol Å⁶)
CF₂···CF₂	77172756.95	−7633.897037
CF₃···CF₃	24370344.30	−2410.704328
CF₂···CF₃	50771550.62[g]	−5022.300682[g]

[a] Ref 48. [b] Equilibrium distances between the S atoms and the corresponding three closest Au atoms are different for all S atoms in the unit cell (ref 44). [c] Refs 50 and 51. [d] Ref 52. [e] Ref 53. [f] Ref 54. [g] Taken as the arithmetic mean of the parameters for CF₂···CF₂ and CF₃···CF₃ interactions.

calculations on the Ar + CF₄ system, using focal point CCSD(T) with complete basis set extrapolation.[47]

The UA model of the F-SAM consists of 48 chains of CF₃(CF₂)₇S radicals adsorbed on a single layer of 196 constrained Au atoms. The sulfur atoms of the CF₃(CF₂)₇S moieties are placed 1.931 Å above the Au{111} surface[48] in close-packed rows rotated 30° from the close-packed rows of gold atoms,[44] maintaining the nearest-neighbor chain−chain distance of 5.776 Å. The backbone of the CF₃(CF₂)₇S radical has a tilt angle of 9° with respect to the Au surface normal, which is in quite good agreement with the experimental value of $12 \pm 2°$,[44] and shows the typical helical conformation of perfluorocarbon chains.[49]

As for the EA model, the general expression of the potential energy of the UA F-SAM surface follows eq 3, but the nonbonded interactions are represented by Lennard-Jones 6-12 potentials instead of Buckingham functions

$$V^{NB}(r_{ij}) = \frac{A_{\alpha\beta}}{r_{ij}^{12}} + \frac{B_{\alpha\beta}}{r_{ij}^{6}} \qquad (8)$$

Within a chain, nonbonding interactions for united atoms separated by four or more bonds were fully included in the potential energy evaluation. Lennard-Jones interactions between united atoms separated by one, two, and three bonds were neglected. The values of the force-field parameters employed in the UA model of F-SAM were taken from the literature[50−54] and are collected in Table 1. A spherical potential truncation at

13.5 Å and no tail corrections were used in the UA F-SAM model.

The Ar/F-SAM interaction function ($V_{Ar,surf}$) for the UA model was derived from a fit of the Buckingham expression to a potential, $V_{av}(R)$, obtained by isotropically averaging the EA interactions in the Ar···CF₄ system[46]

$$V_{av}(R) = \frac{1}{n} \sum_{k=1}^{n} \sum_{i} V_R(r_{i,Ar}; \theta_k, \varphi_k, \chi_k) \qquad (9)$$

where R is the Ar···C separation, n is the number of random orientations of CF₄ (defined in terms of the Euler angles θ_k, φ_k, and χ_k) for a given distance R, and $V_R(r_{i,Ar}; \theta_k, \varphi_k, \chi_k)$ is the EA potential energy of Ar···CF₄. At constant R, the value of this potential energy varies with the orientation of CF₄, which determines the $r_{i,Ar}$ distances (i stands for C or F in CF₄). The parameters for both the EA and UA $V_{Ar,surf}$ interaction functions are reported in ref 46.

B. Trajectory Simulations. Trajectory initial conditions were chosen appropriately in order to mimic the experimental conditions. The angle with respect to the surface normal for the Ar projectile, that is, the incident polar angle (θ_i), was 30°. The orientation of the projection of the initial Ar velocity vector onto the F-SAM surface, given by the initial azimuthal angle (χ_i), was chosen randomly between 0 and 360° to take account of all possible collisions with different chain orientations on the surface. The points on the surface at which the Ar atom impacts were randomly selected from the central unit cell of the surface, defined by the vectors $\vec{u}$ and $\vec{v}$ determined from the Cartesian coordinates of the terminal carbon atoms for three chains at the corner of the unit cell. The aiming point ($\vec{A}$) in the unit cell was randomly calculated by

$$\vec{A} = R_1\vec{u} + R_2\vec{v} \qquad (10)$$

where R_1 and R_2 are two freshly generated random numbers. Periodic boundary conditions and the image vector convention[55] were used to model a larger surface, which is especially important for collisions leading to physisorption and multiple Ar encounters with the surface.

Ensembles of 2000 trajectories were run at collision energies (E_i) of 50 and 100 kJ/mol, employing the VENUS05 program.[56] The initial separation between the Ar atom and the surface aiming point was 30 Å (38 Å above the gold atoms). The integration of the classical equations of motion was performed with a fixed step size of 0.3 fs using the Adams−Moulton algorithm. Prior to the propagation of the first trajectory, a molecular dynamics simulation was carried out for 2 ps to attain thermal relaxation of the F-SAM surface at 295 K. The structure thus obtained was used later as the initial structure of a 100 fs equilibration run before the second trajectory. This process was repeated before initiation of each trajectory.

Trajectories were halted when the separation between Ar and the surface reached 35 Å or when 60 ps had elapsed. Then, several properties were evaluated from the atomic Cartesian coordinates and momenta, such as the final translational energy of Ar, the final internal energy of the surface, the residence time of Ar (τ_{res}) on/in the surface, and the angular distributions of the scattered Ar atoms.

For some trajectories [1.2 (15%) and 0.6% (5%) for the EA (UA) model at 50 and 100 kJ/mol, respectively], the Ar atom did not desorb within the integration time of 60 ps. Of these percentages of incomplete trajectories, ~90% correspond to penetrating trajectories. One may expect that, after this period of time, the Ar atom reached thermal equilibrium with the

F-SAM surface. Eventually, the Ar atom will desorb from the surface, presumably following a statistical distribution of velocities. Accordingly, for these trajectories, the final Ar velocity was randomly assigned from a 295 K Boltzmann distribution, θ_f was randomly sampled from a cosine distribution, and χ_f was sampled uniformly within the range of $0-360°$.

C. Experimental Approach. The scattering experiments were conducted using an alkanethiol SAM created by immersion of a gold-coated silica substrate in a 1 mM ethanolic solution of $CF_3(CF_2)_7(CH_2)_2SH$ for 48 h. Although the degree of fluorination of the alkane chains employed in the experiments was slightly lower than that used in the simulations, previous work has demonstrated that only about seven carbon atoms along the individual chains are involved in the energy-transfer event for high-energy Ar collisions on hydrocarbon SAMs.[6] Therefore, the two CH_2 groups buried beneath the SAM are expected to have a minor effect on the overall scattering dynamics. The structure of the monolayer is very similar to that employed in the simulations and has been characterized by Alves and Porter.[57] The resulting monolayer sample was removed from solution, rinsed in ethanol, dried extensively in ultrapure N_2, and then transferred immediately into an ultrahigh-vacuum scattering chamber via a rapid load−lock system. The atomic beam scattering experiments were conducted for high-energy (100 kJ/mol) and low-energy (50 kJ/mol) Ar scattering from the self-assembled monolayer. As described in detail elsewhere, the experiments were performed by directing a nearly mono-energetic Ar atomic beam at the monolayer surface under ultrahigh-vacuum conditions.[4] The peak incident beam energy was controlled using standard seeding techniques.[58] As in the simulations, the incident angle was set to 30° with respect to the surface normal. The flight times of the Ar atoms were recorded as they traveled from a spinning slotted wheel, scattered from the monolayer, and passed through an aperture into a quadrupole mass spectrometer located at the specular angle of 30°. The raw spectrometer signal in the TOF distributions was proportional to the number density, $N(t)$, and was used to compute the probability, $P(E_f)$, that an argon atom leaves the surface with final energy E_f.

III. Simulation Results and Discussion

A. Types of Trajectories. As expected, the simulations show the three limiting types of trajectories, that is, direct, physisorbing, and penetrating, described in the Introduction. Direct trajectories are those having only one inner turning point (ITP) in their motion perpendicular to the surface plane and give rise to inelastic scattering.[32,35] Physisorption is identified as an event in which Ar undergoes two or more ITPs without penetration. On average, physisorption trajectories are adsorbed on the surface during a substantial period of time (several picoseconds). Following the criterion employed in the previous study of CO_2 scattering from the F-SAM,[21] a trajectory is considered as penetrating if the Ar atom approaches within 11.6 Å of the Au surface, which is a height intermediate of the average heights of the C atoms of the $-CF_3$ terminal groups and adjacent $-CF_2-$ groups. The trajectories that penetrated the surface are not delineated by whether the penetration and desorption are direct or whether the Ar atom is temporarily trapped on the top of the F-SAM before it penetrates and/or after it leaves the surface interior.

Table 2 shows the percentage of each type of trajectory for the two collision energies investigated (50 and 100 kJ/mol). For the UA model, the percentage of direct scattering increases substantially as the collision energy increases. This contrasts with

TABLE 2: Percentages of Different Trajectory Types

$E_i{}^a$	trajectory types^b					
	direct		penetrate		physisorb	
	UA	EA	UA	EA	UA	EA
50	27	47	23 (2;21)	9 (6; 3)	50	44
100	48	46	9 (1;8)	17 (14;3)	43	37

^{a} Collision energy in kJ/mol. ^{b} The percentage of direct penetration and physisorption penetration is given in parentheses as (% of direct penetration; % of physisorption penetration).
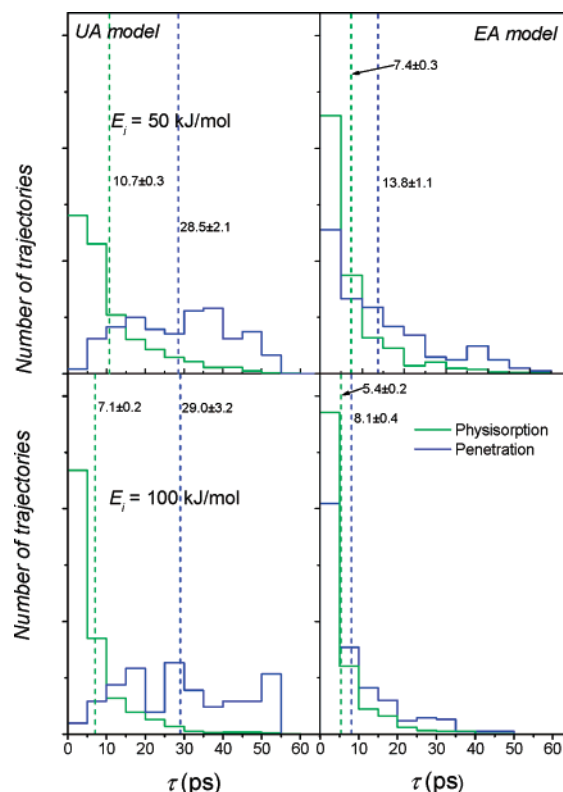

Figure 1. Distributions of residence times for physisorbing and penetrating trajectories calculated with the EA and UA models at 50 and 100 kJ/mol. Vertical dashed lines indicate average values, and the uncertainty is given by the standard deviation of the mean.

the results for the EA model, which show similar percentages of direct scattering for both collision energies. For the UA model, the penetration probability decreases with an increase in E_i, while the opposite effect is found for the EA mode. While the percentage of direct penetration is only $1-2\%$ for the UA model, for the EA model, this percentage is larger ($6-14\%$).

For each trajectory, we evaluated a residence time (τ) as the difference between the times of the last and first ITPs in the perpendicular motion of the Ar atom. With this definition, used recently in the simulations of CO_2 + F-SAM,[21] only penetrating trajectories with more than one ITP and physisorption trajectories will have nonzero residence times. A different criterion based on the time the projectile spends within a specified height above the surface gives short residence times for direct trajectories.[7,11] Figure 1 displays distributions of residence times determined by the ITP approach for the penetrating and physisorbing trajectories. As found for the CO_2 + F-SAM system,[21] the residence times of the penetration events are longer than those of the physisorbing trajectories, especially for the UA model, which shows average values significantly larger than those predicted by the EA model. The shapes of the distributions of residence times obtained with the EA and UA models of the

Scattering Dynamics of Ar from a F-SAM Surface

J. Phys. Chem. A, Vol. 111, No. 49, 2007 **12789**

TABLE 3: Average Translational Energies of the Scattered Ar Atoms[a]

		total		direct		penetrate		physisorb		$(\Delta\chi \approx 0;$ $\theta_f \approx 30)$[b]		exp
						$E_i = 50$						
		UA	EA	UA	EA	UA	EA	UA	EA	UA	EA	
$\langle E_f \rangle$		10.3	16.2	13.4	18.0	5.7	5.1	10.7	16.3	11.7	16.6	11.6
						$E_i = 100$						
		UA	EA	UA	EA	UA	EA	UA	EA	UA	EA	
$\langle E_f \rangle$		23.0	25.7	23.4	27.3	5.6	8.0	25.9	32.0	24.7	24.8	21.6

[a] Energy is in kJ/mol. [b] For these trajectories, $\Delta\chi = \pm 40$, and the final scattering angle is $\theta_f = 30 \pm 20$, resembling the experimental conditions ($\Delta\chi = 0$ and $\theta_f = 30$).

F-SAMs are also different. The differences between the EA and UA models of the F-SAM results found in this study are discussed in more detail in section III.D.

Also, the average residence time decreases as E_i increases, except for the penetrating trajectories calculated with the UA model. For physisorption, all of the $P(\tau)$ distributions peak at $\tau = 0$ and decrease with increasing τ, following an exponential-like pattern (see Figure 1). The $P(\tau)$ also peaks at $\tau = 0$ for the EA, but not the UA, penetrating trajectories.

B. Energy Transfer. Table 3 collects the final average translational energy of the scattered Ar atoms for the 50 and 100 kJ/mol collision energies. The average energies transferred to the surface (ΔE_{surf}) can be evaluated by energy conservation as $E_i - E_f$. The results obtained in the present work resemble those of the previous study on $CO_2 + $ F-SAM.[21] For example, the percentage of the incident energy transferred to vibrational modes of the surface is substantial. Specifically, for the EA model, we found in this study that $\langle \Delta E_{surf} \rangle$ is 68% (74%) for $E_i = 50$ kJ/mol (100 kJ/mol) when all trajectories are considered in the averaging. For the UA model, the percentages are 79 and 77% for the 50 and 100 kJ/mol collisions, respectively. For both the EA and UA models, the results for the direct trajectories are quite similar to those obtained for the physisorbing trajectories. At 50 kJ/mol, the physisorbing trajectories lead to somewhat more energy transfer than do direct collisions, but strikingly, the contrary is found at $E_i = 100$ kJ/mol. For the penetrating trajectories, the fraction of the collision energy transferred to the surface is very large, as expected.

The distributions of the final translational energy of the Ar atom, $P(E_f)$, for the different classes of trajectories are depicted in Figure 2 as fits using the method of Legendre moments.[59] The $P(E_f)$ for the direct trajectories are quite broad and have a single peak. For the physisorbing trajectories, the $P(E_f)$ display a bimodal pattern. The $P(E_f)$ for the physisorbing and penetrating trajectories show a well-defined peak at small E_f, and particularly for the penetrating distributions, the peak is quite marked, indicating efficient accommodation of the final translational energy. Except for penetration, all of the distributions become broader as the collision energy increases. All of these trends were also found in the related system $CO_2 + $ F-SAM.[21]

The low-energy region of the $P(E_f)$ distributions was fit to a Maxwell−Boltzmann distribution for thermal desorption (eq 1), but following previous studies,[7,10−13] in this work, the temperature of the distribution (T_s) was treated as a variable. This low-energy region of the curve (fit to a Boltzmann distribution) is called the Boltzmann component. The fits to eq 1 for the total number of trajectories are shown in Figure 3. The parameters obtained from these fits, as well as those derived from similar fits for the penetrating and physisorbing trajectories, are
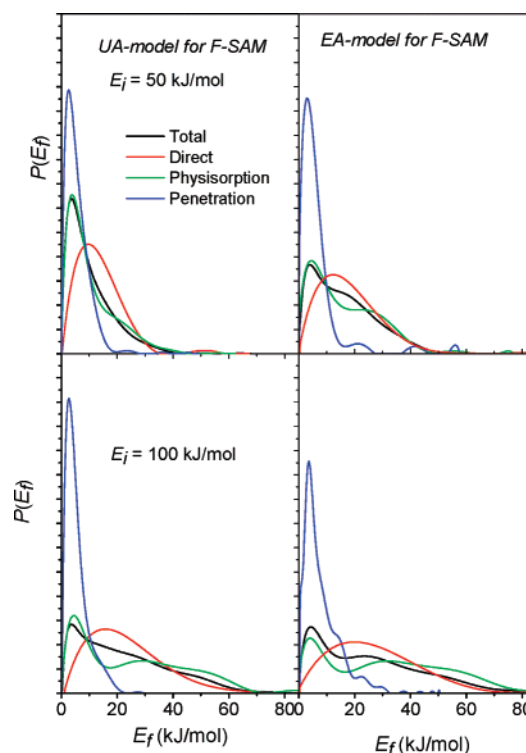

Figure 2. Translational energy distributions $P(E_f)$ of the scattered Ar atoms for direct, physisorbing, penetrating, and total trajectories, depicted as fits by the method of Legendre moments.[59] The distributions were calculated with the UA (left panels) and EA (right panels) models, at 50 (upper panels) and 100 kJ/mol (lower panels). All distributions were normalized.
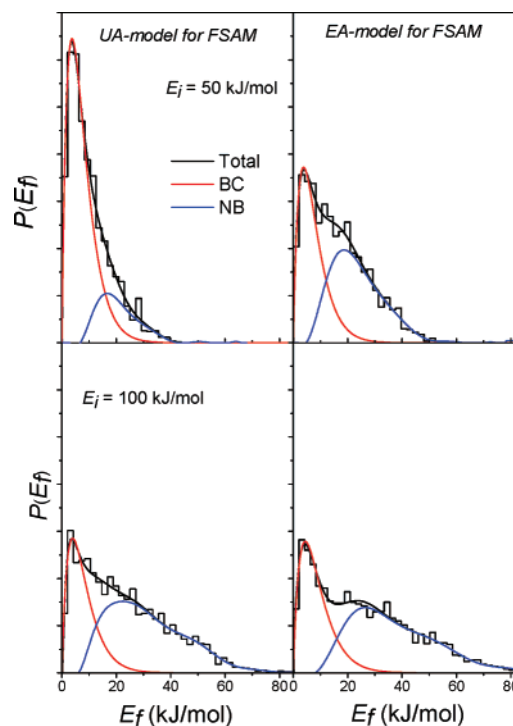

Figure 3. Translational energy distributions $P(E_f)$ of the total scattered Ar atoms, and Boltzmann (BC) and non-Boltzmann (NB) components in the $P(E_f)$ distributions (see text). The $P(E_f)$ distributions are plotted as histograms and as fits by the method of Legendre moments (black curve).[59]

collected in Table 4. These parameters may serve as a guide to estimate the degree of thermal equilibration experienced by the projectile upon interaction with the surface. The direct collisions

12790 *J. Phys. Chem. A, Vol. 111, No. 49, 2007*

Vázquez et al.

TABLE 4: Parameters for the Boltzmann Fits to the $P(E_f)$ Distributions[a]

E_i	total		penetrate		physisorb	
	UA	EA	UA	EA	UA	EA
50	0.78; 447	0.46; 454	1.00; 338	0.98; 331	0.81; 454	0.61; 557
100	0.37; 475	0.40; 528	1.00; 314	0.95; 425	0.46; 531	0.30; 471

[a] The first number in each pair is the fraction of the Boltzmann component in the fit and the second is the temperature (K) for the Boltzmann component. The collision energy is in kJ/mol.

do not lead to Boltzmann distributions. For the total and physisorption trajectories, the Boltzmann component decreases as E_i increases, which is consistent with a higher difficulty in thermal accommodation as the collision energy increases. However, for the penetrating trajectories, the Boltzmann component fraction is unity or near unity and insensitive to E_i. The fitted temperature of the Boltzmann component for the penetrating $P(E_f)$ distributions is only slightly larger than the surface temperature of 295 K, except the 425 K temperature for the EA model at $E_i = 100$ kJ/mol, which points out that thermal accommodation of the final translational energy is accomplished to a large degree. For the physisorbing trajectories and the total trajectories, the fitted temperature is substantially larger than the surface temperature. This result, in which the Boltzmann components show temperatures significantly higher than the surface temperature, has been found in previous work[7,10,13,21] and suggests that there is sufficient relaxation to form a Boltzmann distribution with a subset of modes of the surface but insufficient accommodation for the scattered Ar atoms to acquire the surface temperature.[13]

C. Angular Distributions of the Scattered Ar Atoms. For each collision energy, we analyzed the distributions of the angles formed between the final Ar velocity vector and the surface normal (θ_f). These scattering angle distributions, $P(\theta_f)$, are displayed in Figure 4, and the average scattering angles, $\langle \theta_f \rangle$, are shown in Table 5. The dashed line in the figure is the expected distribution for random scattering ($\sin \theta \cos \theta$).[11] In only one plane perpendicular to the surface, the random distribution is given by $\cos \theta$.[54] As can be seen, if we analyze separately the direct, physisorbing, and penetrating trajectories, we observe clear differences between the corresponding distributions and average angles. As expected, the distributions for penetrating trajectories are more random than are the distributions for direct scattering (shifted toward lower θ_f) and physisorption (shifted toward higher θ_f). At first sight, one may expect random distributions for physisorption trajectories. However, in our analysis, these types of trajectories also include a significant fraction with a small number of ITPs (see Figure 5) which do not thermalize significantly. Actually, we found that by increasing the number of ITPs for a trajectory to be identified as a physisorption type, the average scattering angle approaches 45°, the value for random scattering. Interestingly, when all of the trajectory types are grouped together, the distributions follow the pattern for random scattering quite well, especially those of the EA model. As a result, the corresponding average scattering angles are close to 45°.

Figure 6 shows the distributions of the change in the azimuthal angle $\Delta\chi = \chi_f - \chi_i$, that is, the angle formed between the projections of the initial and final Ar velocity vectors onto the plane of the surface; $\Delta\chi = 0$ indicates in-plane-forward scattering. The distributions of the total trajectories are fairly symmetric with respect to this plane and peak at, or close to, $\Delta\chi = 0°$ (or $\Delta\chi = 360°$). The UA distributions show somewhat more forward scattering than do the EA distributions. We have
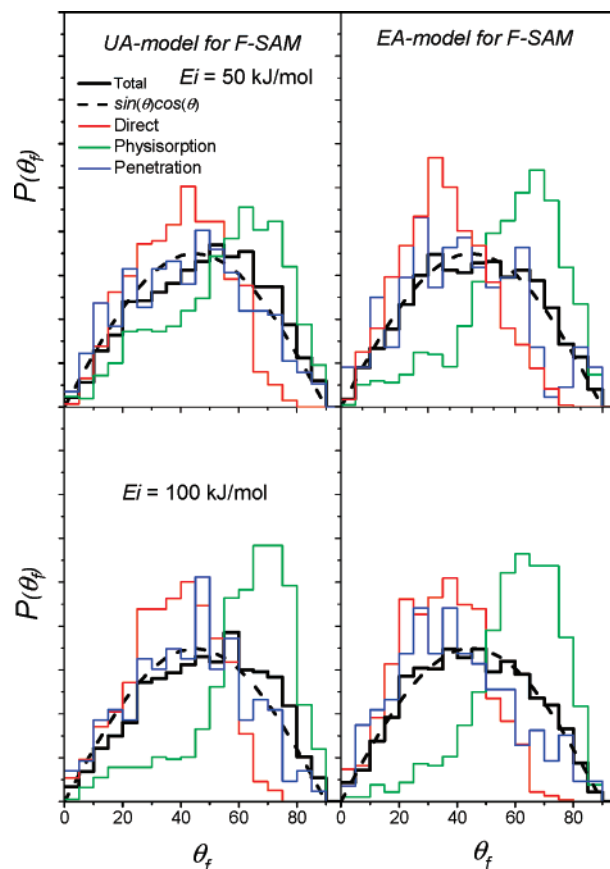
Figure 4. Distributions of the scattering angle for direct, physisorbing, penetrating, and total trajectories. The dashed curve corresponds to random scattering.

TABLE 5: Average Scattering Angles for Different Trajectory Types[a]

E_i	average scattering angle $\langle \theta_f \rangle$[a]							
	direct		penetrate		physisorb		total	
	UA	EA	UA	EA	UA	EA	UA	EA
50	39.9	36.1	43.5	41.7	55.1	58.2	48.3	46.2
100	37.8	34.7	43.2	39.6	61.2	60.4	48.5	45.0

[a] Energies are given in kJ/mol and angles in degrees. The incident collision angle θ_i is 30°.

also analyzed these distributions for the different trajectory types. As can be seen, for the direct and physisorbing trajectories, the distributions are peaked in the in-plane-forward direction, while for the penetrating trajectories, the distributions are more random. These trends were also predicted for collisions of Ar with alkanethiolate SAMs.[8,15] The result that the physisorption trajectories have azimuthal angle distributions peaking in the in-plane-forward direction is not surprising, taking into account that a significant fraction of these trajectories does not thermalize, as discussed above.

D. Comparison between the Simulation Models. The present study shows that, in general, the UA model leads to results in reasonably good agreement with those obtained by the more CPU-time-demanding EA model, although in some cases, the discrepancies are significant. For example, the residence times of penetrating trajectories calculated with the UA model are markedly longer than those predicted with the EA model. In addition, there is a substantial discrepancy between the percentages of direct trajectories calculated at 50 kJ/mol with the EA and UA models, although at 100 kJ/mol, the
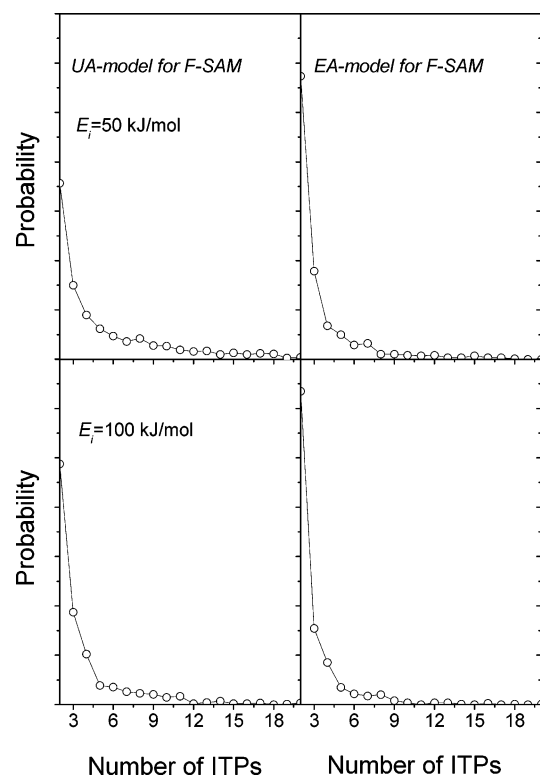
Scattering Dynamics of Ar from a F-SAM Surface

J. Phys. Chem. A, Vol. 111, No. 49, 2007 **12791**

Figure 5. Distribution of the number of inner turning points (ITPs) for the physisorption trajectories.
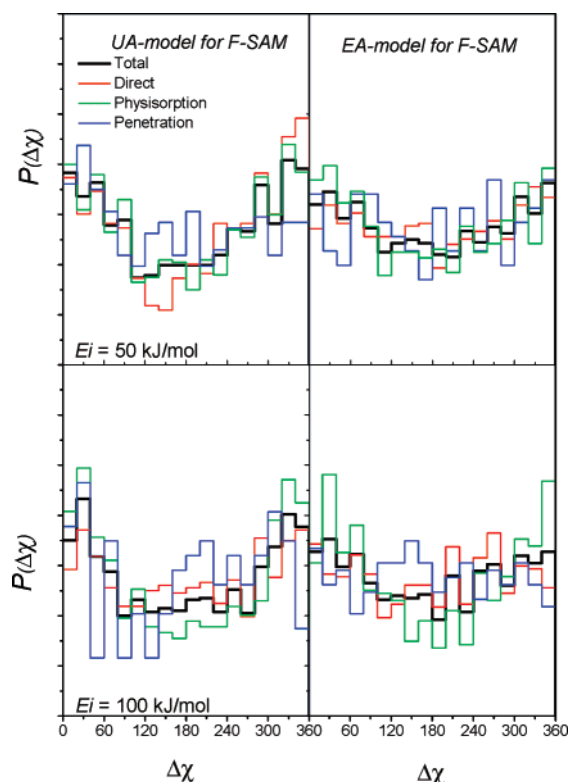

Figure 6. Distributions of the change in the azimuthal angle for direct, physisorbing, penetrating, and total trajectories.

corresponding percentages are similar. This better agreement found at the highest collision energy also occurs for energy transfer. At 50 kJ/mol, energy transfer in the EA model is 12% less efficient than that in the UA model, but this percentage reduces to 3% at $E_i = 100$ kJ/mol. A similar result was found for energy transfer in simulations of Ne with alkanethiol

SAMs.[12] Specifically, energy transferred to the EA surface was approximately 10% smaller than that transferred to the UA surface. The results were explained in terms of a denser and stiffer EA model.[12] The relatively less stiff structure of the UA model absorbs the collision energy more easily by conformational changes than does the EA model. The role of surface stiffness in rationalizing the relative efficiencies of energy transfer in collisions of Ar with H-SAM and F-SAM surfaces is considered in the next section.

The nonbonded interactions between the chains in the monolayer are responsible for the density and stiffness of the models used to represent the surfaces. A decrease in the nonbonded interactions between the chains should make the chains more loosely packed, thus decreasing the barriers to conformational change and favoring the efficiency of energy transfer to the surface.

To make sure that the nonbonded interactions are responsible for the discrepancies between the EA and UA models of the F-SAM surface, we ran additional trajectory calculations for collisions of Ar with a single, isolated chain, and therefore without interchain interactions. In this simulation, the Ar atoms were aimed at the carbon atom of the terminal CF_3 group. Obviously, only direct trajectories took place. The results for $E_i = 100$ kJ/mol show that energy transfer to the UA model is 9% less efficient than that to the EA model. The same result is found when Ar collides with C_2F_6, modeled either by EA or UA potentials; in this case, at $E_i = 100$ kJ/mol, the energy-transfer efficiency is 14% higher for the EA model. These results may be rationalized by the higher number of degrees of freedom in the EA models and also by the higher energy-transfer efficiency to low-frequency modes.

However, at $E_i = 100$ kJ/mol, the energy-transfer efficiencies for the EA and UA models of F-SAM are quite similar to each other, with the efficiency for the latter slightly higher by 2.7%. Therefore, the more efficient energy transfer predicted for the UA model at 50 kJ/mol can be associated with the less stiff nonbonded interactions in the UA model of F-SAM, which compensate the lower number of degrees of freedom in this model.

E. Mass and Surface Stiffness Effects for Energy Transfer to Hydrogenated and Fluorinated Surfaces. Classical trajectory simulations of Ar collisions with *n*-alkanethiol self-assembled monolayer (H-SAM) surfaces at $E_i = 80$ kJ/mol, $T_s = 300$ K, and $\theta_i = 30°$ predict a percentage of energy transfer of about 90% (the exact value varies slightly with the potential model employed in the calculations).[14] Comparing this result with ours, we conclude that, although the amount of energy transferred to the surface is considerable for collisions of Ar with the F-SAM at the conditions explored in this work, fluorination of the alkanethiol chains leads to a significant decrease in the efficiency of energy transfer. This is in line with the early investigation of Cohen et al.,[2] who measured translational energy transfer from He, Ar, and two diatomics (O_2 and NO) to *n*-octadecyltrichlorosilane (OTS) and perfluorinated acid ester (PFAE) monolayers on glass at a collision energy of ∼6 kJ/mol. For Ar (He) collisions, they found that the percentages of energy transferred to the SAM were 4 ± 10% (28 ± 10%) for PFAE and 29 ± 10% (43 ± 10%) for OTS. They rationalized the different efficiencies in energy transfer by the mass ratios of the projectile gas and the surface unit (taken to be either CF_3 or F) and by the rigidity of the surface. The results for collisions of He and Ar with PFAE, however, cannot be easily explained by only these two arguments since the mass ratio should favor energy transfer for Ar collisions.

The importance of the mass ratio in gas-surface scattering dynamics is well documented in the literature.[60−62] Here, to investigate its role in the relative efficiencies of energy transfer in collisions of Ar with the F-SAM and H-SAM surfaces, we performed two different simulations. For one, we calculated the percentage of energy transfer for gas-phase collisions of Ar with CF_3CF_3 and with CH_3CH_3, employing the EA model potentials used in this study. The collisions were for zero impact parameter, with the molecule randomly rotated and a relative collision energy of 100 kJ/mol. We intentionally used the same parameters for fluorine and for hydrogen (i.e., the only difference is in the masses of F and H) because this allows us to analyze energy-transfer changes caused by pure mass effects. The second simulation was the same as that above for Ar + F-SAM, with the EA model and $E_i = 100$ kJ/mol, except the masses of the fluorine atoms were changed to that for a hydrogen atom. Thus, the potential energy function and parameters were the same as those for Ar + F-SAM, and the simulations only investigated a possible mass effect. This latter simulation is identified as Ar + H/F-SAM.

For the Ar + CF_3CF_3 and CH_3CH_3 collisions at 100 kJ/mol, 86 and 82% of the collision energy was transferred to CF_3CF_3 and CH_3CH_3, respectively. Thus, as expected, we found that less energy is transferred when the mass of fluorine is replaced by the mass of hydrogen, for which the mismatch in masses is higher. Also as expected, if the mass of the Ar atom is replaced by that of He, energy transfer becomes more efficient for collisions with CH_3CH_3. Thus, for the gas-phase Ar + CF_3CF_3 and CH_3CH_3 collisions, energy transfer is more efficient to the fluorinated molecule in contrast to what is found for Ar collisions with the F-SAM and H-SAM surfaces. For the Ar + H/F-SAM simulations, we found that the percentage of energy transfer to the surface was 90%, in comparison to the 74% found for Ar + F-SAM. Thus, this simulation reproduced the experimental and simulation findings[5,14] that the hydrogenated SAM absorbs more energy than does the fluorinated one. In fact, the energy-transfer percentage for the Ar + H/F-SAM simulation is in good agreement with the results of ref 14 for Ar + H-SAM and suggests that the overriding factor for energy transfer to the SAM is the mass effect and not the potential energy function since it is different for the H-SAM and H/F-SAM.

Before discussing the different mass effect found for the Ar + CH_3CH_3 and CF_3CF_3 simulations, as compared to those for Ar + F-SAM and H/F-SAM, the energy-transfer pathways for these two sets of simulations should be discussed. For the gas-phase Ar collisions with CH_3CH_3 and CF_3CF_3, the translational to vibrational (T → V) energy transfer is to the intramolecular modes of the two molecules. However, for the Ar + F-SAM and H/F-SAM collisions, the T → V energy transfer may occur to the intramolecular modes of the alkyl chains and/or the interchain intermolecular modes. Previous studies[7,9,13,67] indicate that the latter is the predominant pathway for energy transfer to SAM surfaces. The ability of UA models to describe energy transfer to SAM surfaces, as found here, indicates the importance of energy transfer to the intermolecular modes as compared to that to the intramolecular modes.[5,7,12] Apparently, the determining factor that governs the relative efficiencies of energy transfer in collisions of Ar with F-SAM and H-SAM surfaces is the mobility of the alkyl chains[2] and the ease with which the intermolecular modes may be excited. Because of the heavy mass of the alkyl chains for the F-SAM as compared to that for the H-SAM, the chains of the latter may be more mobile and receptive of the collision energy. This effect of decreased
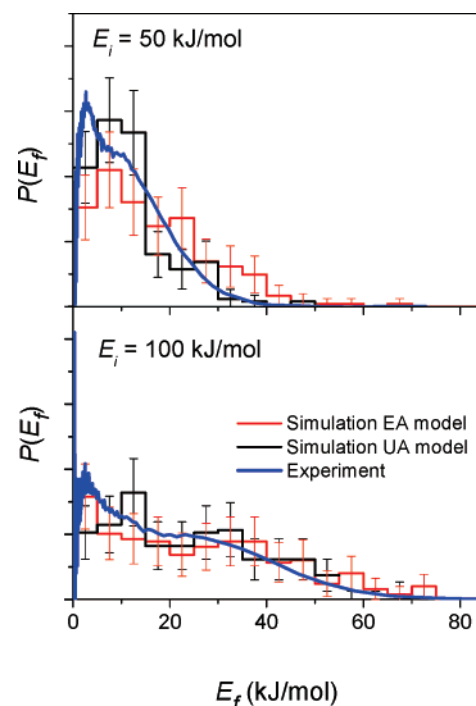

Figure 7. Comparison of the final translational energy distributions obtained by the trajectory simulations and experiment.

collisional energy transfer with a decrease in surface flexibility is consistent with a study of the Ne + H-SAM system in which energy transfer for a harmonic, single potential energy minimum model of the H-SAM was compared with that for the complete anharmonic surface model.[13] Energy transfer is less efficient for the former surface. Other factors such as differences in the tilt angles of the chains and the interaction potentials between Ar and the chain units may play minor roles.

IV. Comparison with Experiment

In this work, the distributions of final translational energies of Ar were measured experimentally at $E_i = 50$ and 100 kJ/mol, with an incident angle $\theta_i = 30°$ and a surface temperature of 295 K, thus resembling the initial conditions employed in the trajectory simulations. However, the experimental distributions were determined with the atomic beam and detector in the same plane and 30° from the surface normal. Therefore, in order to make a rigorous comparison with experiment, one should select only those trajectories that were scattered in a very narrow interval around the in-plane-forward direction ($\Delta\chi = 0$) and around a scattering angle $\theta_f = 30°$ for analysis. Because of computational limitations, however, we have had to select all trajectories scattered within a broad interval of $\pm40°$ around the in-plane-forward direction and $\pm20°$ around $\theta_f = 30°$.

The experimental and the simulation results are compared in Figure 7 and Table 3. The experimental average values listed in the table were derived from the experimental distributions of Figure 7. In the figure, the trajectory distributions are displayed as histograms only because the number of trajectories that fulfilled the above constraints for $\Delta\chi$ and θ_f ($\approx$250) was not sufficient to accurately fit the distributions by the method of Legendre moments. The uncertainties in the error bars were calculated for a confidence level of 95%. As seen in the figure, there is reasonably good agreement between the experimental and the trajectory distributions. For the collision energy of 50 kJ/mol, the average translational energy of the scattered Ar atoms (for $\Delta\chi = \pm40°$ and $\theta_f = 30 \pm 20°$) obtained with the

UA model is predicted to be 11.7 kJ/mol, which is in excellent agreement with the experimental result of 11.6 kJ/mol. The average value computed using the EA model is 5 kJ/mol higher. For $E_i = 100$ kJ/mol, the predictions obtained with both the EA and UA models are similar to each other (∼25 kJ/mol for $<E_f>$) and in good agreement with the experimental results (22 kJ/mol).

V. Conclusions

Classical trajectory simulations and atomic beam scattering experiments were performed to explore energy transfer in collisions of Ar with a fluorinated alkanethiol self-assembled monolayer on gold, at incident energies of 50 and 100 kJ/mol. Both explicit-atom and the united-atom model potentials were used to represent the F-SAM surface in the simulations.

The simulations consist of direct inelastic scattering, physisorption, and penetration trajectories, the three types of limiting mechanisms expected for collisions of Ar with the F-SAM surface. The translational energy distributions $P(E_f)$ for the direct collisions have a single peak. By contrast, the physisorbing trajectories have an obvious bimodal $P(E_f)$ distribution. The fitted temperatures of their low-energy Boltzmann components are significantly higher than the surface temperature, which may be interpreted as insufficient accommodation for the scattered atoms to acquire the surface temperature but sufficient to form a Boltzmann distribution with a subset of modes of the surface.[13] All of the $P(E_f)$ distributions, except those associated with penetration, show a clear broadening as E_i increases. By contrast, the $P(E_f)$ for the penetrating trajectories are rather narrow, and their widths do not change significantly with the amount of collision energy, which is clear evidence for efficient accommodation of the final translational energy. In fact, the $P(E_f)$ for the penetrating trajectories can be essentially fit to a single exponential with temperatures quite close to that of the surface.

As expected, the scattering angle distributions associated with penetration are more random than are the distributions for direct scattering and physisorption. The total distributions (i.e., including all types of trajectories) are quite random, with average scattering angles close to 45°. In agreement with previous simulations of Ar scattering from alkanethiol SAMs,[8,15] the total distributions are fairly symmetric with respect to the incident plane and peak at, or close to, $\Delta\chi = 0°$ (or $\Delta\chi = 360°$), thus showing some preference for forward scattering. The distributions for the penetrating trajectories are more random, as expected.

The results of this study show that F-SAM surfaces are less efficient than H-SAM surfaces at dissipating the incident translational energy of the colliding Ar atoms. This may be explained by the tighter structure of the F-SAM in comparison with that of the H-SAM, which makes possible conformational changes of the monolayer chains more difficult. Other factors such as the differences in the tilt angles of the chains, differences in the atomic masses of hydrogen and fluorine, and differences in the interaction potentials between Ar and the unit chains may play minor roles in the relative efficiencies of energy transfer in these systems.

It is of interest that the energy-transfer dynamics for collisions with SAM surfaces is noticeably different from that for metal surfaces[63,64] and more akin to that for organic liquids.[35] The projectile may penetrate the surface,[11,21,65] as found here, and the angle at which it is expelled may depend on the orientation of the SAM chains. The projectile is expelled from the SAM by repulsive interactions[11,65] as the chains realign and return to their equilibrium positions, and the translational energy of the expelled projectile may increase with the deepness of its penetration. A "washboard" model[66] often represents scattering with metal surfaces, but to describe the flexibility of softer, more highly corrugated surfaces such as SAMs, a "washboard with moment of inertia" model is needed.[67] For Ar + Pt(111) scattering,[68] there is rapid thermalization of the normal component of the scattered projectile's velocity but quite slow thermalization (80−100 ps) of the parallel component. For Ne and Ar scattering of H-SAM surfaces,[5,7] there are much smaller differences between the times of thermalization of the normal and parallel velocity components. The former's is thermalized in <2 ps, while the latter's is only slightly longer (4−8 ps). It is postulated that efficient thermalization of the parallel component for scattering off of a SAM arises from a combination of interchain wagging modes of appropriate frequency and the highly corrugated surface.[7]

The translational energy distributions of the scattered Ar atoms, $P(E_f)$, predicted by the Ar + F-SAM trajectory simulations are in reasonably good agreement with those determined experimentally. This, together with the accumulated experience of research on scattering of gases with SAM surfaces, points out that the simulation models employed in this study are reliable for studying the dynamics of energy transfer in collisions of Ar with F-SAMs, at least from a qualitative point of view. In general, the results obtained with the UA model agree quite well with those predicted by the EA model. For several properties, however, the agreement is not as good. For example, the residence times of penetrating trajectories predicted with the UA model are much longer than the corresponding times obtained with the EA model. Also, the percentage of direct trajectories calculated at 50 kJ/mol with the UA model is substantially lower than that computed with the EA model. Related to this is the more efficient energy transfer of the UA model in comparison with the EA model, which was also found in energy-transfer simulations of Ne with alkanethiol SAMs.[12] To a large extent, the disagreement between the UA and EA results may come from differences in the stiffness of the UA and EA potentials due to different nonbonding potentials between the chains. The former model potential, being less stiff, favors the efficiency of energy transfer due to less impediments to conformational changes. Future work may be needed to improve the quality of the UA model.

References and Notes

(1) Love, J. C.; Estroff, L. A.; Kriebel, J. K.; Nuzzo, R. G.; Whitesides, G. M. M. *Chem. Rev.* **2005**, *105*, 1103.

(2) Cohen, S. R.; Naaman, R.; Sagiv, J. *Phys. Rev. Lett.* **1987**, *58*, 1208.

(3) Paz, Y.; Naaman, R. *J. Chem. Phys.* **1991**, *94*, 4921.

(4) Day, B. S.; Shuler, S. F.; Ducre, A.; Morris, J. R. *J. Chem. Phys.* **2003**, *122*, 8084.

(5) Gibson, K. D.; Isa, N.; Sibener, S. J. *J. Chem. Phys.* **2003**, *119*, 13083.

(6) Day, B. S.; Morris, J. R. *J. Phys. Chem. B* **2003**, *107*, 7120.

(7) Isa, N.; Gibson, K. D.; Yan, T.; Hase, W. L.; Sibener, S. J. *J. Chem. Phys.* **2004**, *120*, 2417.

(8) Day, B. S.; Morris, J. R. *J. Chem. Phys.* **2005**, *122*, 234714.

Vázquez et al.

(9) Yan, T.; Hase, W. L. *J. Phys. Chem. A* **2001**, *105*, 2117.

(10) Yan, T.; Hase, W. L.; Barker, J. R. *Chem. Phys. Lett.* **2000**, *329*, 84.

(11) Yan, T.; Hase, W. L. *Phys. Chem. Chem. Phys.* **2000**, *2*, 901.

(12) Yan, T.; Hase, W. L. *J. Phys. Chem. B* **2002**, *106*, 8029.

(13) Yan, T.; Isa, N.; Gibson, K. D.; Sibener, S. J.; Hase, W. L. *J. Phys. Chem. A* **2003**, *107*, 10600.

(14) Day, B. S.; Morris, J. R.; Troya, D. *J. Chem. Phys.* **2005**, *122*, 214712.

(15) Day, B. S.; Morris, J. R.; Alexander, W. A.; Troya, D. *J. Phys. Chem. A* **2006**, *110*, 1319.

(16) Shuler, S. F.; Davis, G. M.; Morris, J. R. *J. Chem. Phys.* **2002**, *116*, 9147.

(17) Ferguson, M. K.; Lohr, J. R.; Day, B. S.; Morris, J. R. *Phys. Rev. Lett.* **2004**, *92*, 073201.

(18) Li, G.; Bosio, S. B. M.; Hase, W. L. *J. Mol. Struct.* **2000**, *556*, 43.

(19) Troya, D.; Schatz, G. C. *J. Chem. Phys.* **2004**, *120*, 7696.

(20) Tasić, U.; Yan, T.; Hase, W. L. *J. Phys. Chem. B* **2006**, *110*, 11863.

(21) Martínez-Núñez, E.; Rahaman, A.; Hase, W. L. *J. Phys. Chem. C* **2007**, *111*, 354.

(22) Wainhaus, S. B.; Lim, H.; Schultz, D. G.; Hanley, L. *J. Chem. Phys.* **1997**, *106*, 10329.

(23) Schultz, D. G.; Wainhaus, S. B.; Hanley, L.; de Sainte Claire, P.; Hase, W. L. *J. Chem. Phys.* **1997**, *106*, 10337.

(24) Laskin, J.; Futrell, J. H. *J. Chem. Phys.* **2003**, *119*, 3413.

(25) Meroueh, O.; Hase, W. L. *J. Am. Chem. Soc.* **2002**, *124*, 1524.

(26) Perkins, B. G.; Nesbitt, D. J. *J. Phys. Chem. A* **2007**, *111*, 7420.

(27) Perkins, B. G.; Nesbitt, D. J. *J. Phys. Chem. B* **2006**, *110*, 17126.

(28) Perkins, B. G.; Haber, T.; Nesbitt, D. J. *J. Phys. Chem. B* **2005**, *109*, 16396.

(29) Los, J.; Gleeson, M. A.; Koppers, W. R.; Weeding, T. L.; Kleyn, A. W. *J. Chem. Phys.* **1999**, *111*, 11080.

(30) Koppers, W. R.; Beijersbergen, J. H. M.; Weeding, T. L.; Kistemaker, P. G.; Kleyn, A. W. *J. Chem. Phys.* **1997**, *107*, 10736.

(31) Koppers, W. R.; Gleeson, M. A.; Lourenço, J.; Weeding, T. L.; Los, J.; Kleyn, A. W. *J. Chem. Phys.* **1999**, *110*, 2588.

(32) Saecker, M. E.; Nahanson, G. M. *J. Chem. Phys.* **1993**, *99*, 7056.

(33) Hwang, G. S.; Anderson, C. M.; Gordon, M. J.; Moore, T. A.; Minton, T. A.; Giapis, K. P. *Phys. Rev. Lett.* **1996**, *77*, 3049.

(34) Minton, T. A.; Giapis, K. P.; Moore, T. *J. Phys. Chem. A* **1997**, *101*, 6549.

(35) Nathanson, G. M. *Annu. Rev. Phys. Chem.* **2004**, *55*, 231.

(36) Hurst, J. E.; Becker, C. A.; Cowin, J. P.; Janda, K. C.; Wharton, L. *Phys. Rev. Lett.* **1979**, *43*, 1175.

(37) Rettner, C. T.; Schweizer, E. K.; Mullins, C. B. *J. Chem. Phys.* **1989**, *90*, 3800.

(38) King, M. E.; Nathanson, G. M.; Hanning-Lee, M. A.; Minton, T. K. *Phys. Rev. Lett.* **1993**, *70*, 1026.

(39) Grimmelmann, E. K.; Tully, J. C.; Cardillo, M. J. *J. Chem. Phys.* **1980**, *72*, 1039.

(40) Bertilsson, L.; Potje-Kamloth, K.; Liess, H.-D.; Liedberg, B. *Langmuir* **1999**, *15*, 1128.

(41) Vogt, A. D.; Beebe, T. P. *J. Phys. Chem. B* **1999**, *103*, 8482.

(42) Vogt, A. D.; Beebe, T. P. *Langmuir* **1999**, *15*, 2755.

(43) Borodin, O.; Smith, G. D.; Bedrov, D. *J. Phys. Chem. B* **2002**, *106*, 9912.

(44) Liu, G.-Y.; Fenter, P.; Chidsey, C. E. D.; Ogletree, D. F.; Eisenberger, P.; Salmeron, M. *J. Chem. Phys.* **1994**, *101*, 4301.

(45) Sellers, H.; Ulman, A.; Shnidman, Y.; Eilers, J. E. *J. Am. Chem. Soc.* **1993**, *115*, 9389.

(46) Vayner, G.; Alexeev, Y.; Wang, J.; Windus, T. L.; Hase, W. L. *J. Phys. Chem. A* **2006**, *110*, 3174.

(47) Tasić, U.; Hein, P.; Troya, D. *J. Phys. Chem. A* **2007**, *111*, 3618.

(48) Bosio, S. B. M.; Hase, W. L. *J. Chem. Phys.* **1997**, *107*, 9677.

(49) Sprik, M.; Rothlisberger, U.; Klein, M. L. *Mol. Phys.* **1999**, *97*, 355.

(50) Weiner, S. J.; Kollman, P. A.; Case, D. A.; Singh, U. C.; Ghio, C.; Alagona, G.; Profeta, S.; Weiner, P. *J. Am. Chem. Soc.* **1984**, *106*, 765.

(51) Brooks, B. R.; Bruccoleri, R. E.; Olafson, B. D.; States, D. J.; Swaminathan, S.; Karplus, M. *J. Comput. Chem.* **1983**, *4*, 187.

(52) Hariharan, A.; Harris, J. G. *J. Chem. Phys.* **1994**, *101*, 4156.

(53) Cui, S. T.; Siepmann, J. I.; Cochran, H. D.; Cochran, H. D.; Cummings, P. T. *Fluid Phase Equilib.* **1998**, *146*, 51.

(54) Cui, S. T.; Cochran, H. D.; Cummings, P. T. *J. Phys. Chem. B* **1999**, *103*, 4485.

(55) Allen, M. P.; Tildesley, D. J. *Computer Simulation of Liquids*; Oxford: New York, 1987.

(56) VENUS05 is an enhanced version of VENUS96, with additional algorithms. VENUS96 is available on the website cdssim.chem.ttu.edu and was initially released through the Quantum Chemistry Program Exchange (QCPE) Bulletin, Hase, W. L.; Duchovic, R. J.; Hu, W.; Komornicki, A.; Lim, K. F.; Lu, D.-h.; Peslherbe, G. H.; Swamy, K. N.; Vande Linde, S. R.; Varandas, A.; Wang, H.; Wolf, R. J. *QCPE Bull.* **1996**, *16*, 671.

(57) Alves, C. A.; Porter, M. D. *Langmuir* **1993**, *9*, 3507.

(58) Miller, D. R. *Atomic and Molecular Beam Methods*; Oxford University Press: New York, 1988; Vol. 1, p 14.

(59) Aoiz, F. J.; Bañares, L. *J. Phys. Chem.* **1996**, *100*, 18108.

(60) Goodmann, F. O.; Wachman, H. Y. *Dynamics of Gas-Surface Scattering*; Academic: New York, 1976.

(61) Harris, J. Mechanical Energy Transfer in Particle-Surface Collisions. In *Dynamics of Gas-Surface Interactions*; Rettner, C. T., Ashfold, M. N. R., Eds.; Royal Society of Chemistry: Cambridge, U.K., 1991.

(62) Szabo, T. J.; Siavosh-Haghighi, A.; Adams, J. E. *J. Phys. Chem. B* **2006**, *110*, 1319.

(63) Barker, J. A.; Auerbach, D. J. *Surf. Sci. Rep.* **1985**, *4*, 1.

(64) *The Chemical Physics of Solid Surfaces*: *Surface Dynamics*; Woodruff, D.P., Ed.; Elsevier: Amsterdam, The Netherlands, 2003; Vol. 11.

(65) Gibson, K. D.; Isa, N.; Sibener, S. J. *J. Phys. Chem A* **2006**, *110*, 1469.

(66) Tully, J. C. *J. Chem. Phys.* **1990**, *92*, 680.

(67) Yan, T.; Hase. W. L.; Tully, J. C. *J. Chem. Phys.* **2004**, *120*, 1031.

(68) Head-Gordon, M.; Tully, J. C.; Rettner, C. T.; Mullins, C. B.; Auerbach, D. J. *J. Chem. Phys.* **1991**, *94*, 1516.